A Local Circuit Approach to Understanding Integration of Long-range Inputs in Primary Visual Cortex

David C. Somers, Emanuel V. Todorov, Athanassios G. Siapas, Louis J. Toth, Dae-Shik Kim and Mriganka Sur

Department of Brain and Cognitive Sciences, Massachusetts Institute of Technology, Cambridge, MA 02139, USA

Integration of inputs by cortical neurons provides the basis for the complex information processing performed in the cerebral cortex. Here, we have examined how primary visual cortical neurons integrate classical and nonclassical receptive field inputs. The effect of nonclassical receptive field stimuli and, correspondingly, of long-range intracortical inputs is known to be context-dependent: the same long-range stimulus can either facilitate or suppress responses, depending on the level of local activation. By constructing a large-scale model of primary visual cortex, we demonstrate that this effect can be understood in terms of the local cortical circuitry. Each receptive field position contributes both excitatory and inhibitory inputs; however, the inhibitory inputs have greater influence when overall receptive field drive is greater. This mechanism also explains contrast-dependent modulations within the classical receptive field, which similarly switch between excitatory and inhibitory. In order to simplify analysis and to explain the fundamental mechanisms of the model, self-contained modules that capture nonlinear local circuit interactions are constructed. This work supports the notion that receptive field integration is the result of local processing within small groups of neurons rather than in single neurons.

Introduction

Central to an understanding of cortical function is the question of how cortical neurons integrate inputs to produce outputs. In primary visual cortex (V1), the spatial extent of integration by a neuron includes not only its 'classical' receptive field (RF), where visual stimuli elicit spike responses (presumably through thalamocortical axons), but also the 'nonclassical' receptive field, where stimuli largely modulate responses evoked by other stimuli (presumably via long-range intracortical or inter-areal axons) (Maffei and Fiorentini, 1976; Rockland and Lund, 1982; Gilbert and Wiesel, 1983; T'so et al., 1986; Gilbert, 1992).

The enigmatic nature of this long-range modulation has only recently begun to be understood. Long-range (>1.5 mm) intracortical connections arise almost exclusively from excitatory neurons (Rockland and Lund, 1982; Gilbert and Wiesel, 1983) and make ~80% of their synapses onto excitatory neurons (Kisvarday et al., 1986; McGuire et al., 1991). Not surprisingly, moderate electrical stimulation of long-range inputs generates excitatory postsynaptic potentials (PSPs). Visual stimulation of the far surround, without a central stimulus, can also elicit excitatory responses (Maffei and Fiorentini, 1976; Knierim and Van Essen, 1992). In contrast, experiments in which surround or contextual stimuli (which engage long-range inputs) are added to strong central stimuli indicate a suppressive role for long-range inputs (Blakemore and Tobin, 1972; Nelson and Frost, 1978; Gulyas et al., 1987; Born and Tootell, 1991; Knierim and Van Essen, 1992; Grinvald et al., 1994). Similarly, strong inhibitory PSPs can be induced by electrical stimulation of long-range inputs, provided that the local circuitry is strongly activated (Hirsch and Gilbert, 1991; Weliky et al., 1995). We

(Toth et al., 1996) and others (Roig et al., 1996; Levitt and Lund, 1997; Polat et al., 1998; Sengpiel et al., 1998) have shown that the contrast of the center stimulus regulates whether long-range interactions are facilitative or suppressive: the same surround stimulus facilitates responses when center contrast is low but suppresses responses when center contrast is high (see Fig. 1Aa,b). Surround modulation of responses to preferred orientation stimuli in the classical RF tend to exhibit the strongest suppression (for high-contrast centers) and strongest facilitation (for low-contrast centers) when the surround stimulus is parallel or iso-orientated with the center (Nelson and Frost, 1978, 1985; Knierim and Van Essen, 1992; Sillito et al., 1995; Weliky et al., 1995; Toth et al., 1996; Polat et al., 1998).

Interestingly, similar contrast-related response modulation has also been observed *within* the classical receptive field. Increasing the contrast of a stimulus in the receptive field can, at high contrast, actually cause responses of many V1 cells to decline or 'supersaturate' (Li and Creutzfeldt, 1984; see Fig. 1B). This effect has been observed at contrast levels for which lateral geniculate nucleus (LGN) responses have not saturated or supersaturated (Albrecht and Hamilton, 1982; Bonds 1991). A related phenomenon concerns the receptive field length of end-stopped cells. These cells typically respond maximally to high-contrast stimulus bars of a certain length (and orientation), and responses decline for longer bars (e.g. Hubel and Wiesel, 1965), presumably due to encroachment of the stimulus on inhibitory zones located at the ends of excitatory regions. End-zones have maximal inhibitory effect when activated by stimuli of the preferred orientation (Orban et al., 1979; DeAngelis et al., 1994). However, these inhibitory zones can become excitatory as stimulus contrast is decreased (Jagadeesh and Ferster, 1990; Jagadeesh, 1993), so that low-contrast (preferred orientation) bars have longer optimal lengths than do high-contrast bars (see Fig. 1C).

Common to the phenomena above is the finding that receptive field influences that are net excitatory when the classical receptive field is activated by a low-contrast stimulus become inhibitory when the classical receptive field is activated by a high-contrast stimulus. Paradoxically, both the excitatory and inhibitory effects tend to be strongest for modulatory stimuli aligned at the preferred orientation for the classical RF. These changes in RF sign contradict traditional ideas that assume that the single neuron is the 'unit' of receptive field integration (e.g. Hartline, 1940; Kuffler, 1953; Movshon et al., 1978; Jones and Palmer, 1987; DeAngelis et al., 1995), although these data might be reconciled by invoking dramatic state changes in local neurons or in long-distance synapses. Here we show that local cortical circuitry is sufficient to explain these receptive field 'switching' effects, provided that some contrast-related asymmetry between local cortical excitatory and inhibitory neurons exists. Two different asymmetries are demonstrated:
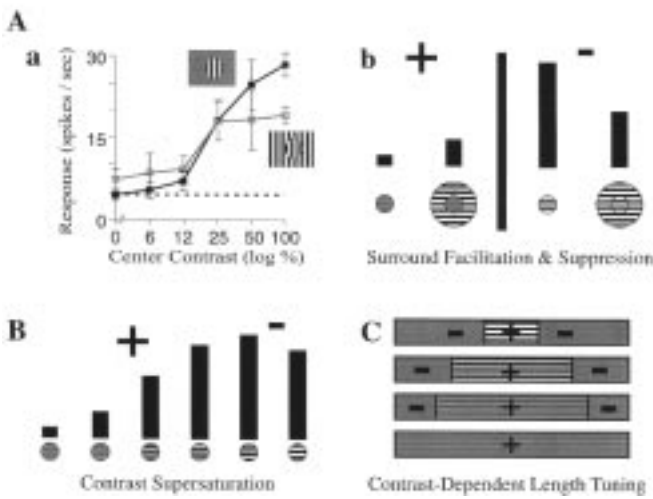
Figure 1. Receptive field influences shifting from excitatory to inhibitory as central stimulus contrast increases. (A) A high-contrast surround stimulus facilitates the response of a low-contrast center stimulus, but the same surround stimulus suppresses responses when the center stimulus is of high contrast. Both facilitation and suppression effects tend to be strongest for iso-orientation surrounds. (a) Typical data from a cell in cat V1 obtained by Toth et al. (1996) but presented here for the first time. Increasing the contrast of an optimally oriented grating stimulus (presented to the classical receptive field in conjunction with a neutral surround) produced typical saturating contrast response functions. All gratings were shown at preferred orientation, direction and velocity, and all responses are averages of 12 stimulus repetitions, randomly interleaved. Central grating stimuli were presented again in conjunction with a high-contrast iso-orientation surround grating. Only the contrast of the central grating was changed. Resulting contrast response functions (CRFs) for the composite stimulus were higher at low center contrasts and lower at high center contrasts than center-only CRFs. Black line represents response to center only stimulation, gray line represents response to full-field stimulation. (b) Schematic representation of surround facilitation and suppression (after Toth et al., 1996; see text for other references). On average (n = 30 cells), responses to the surround stimulus alone (minus background response) were 6.8% of the responses to the optimal center stimulus. But this surround combined with the optimal center grating, on average, suppressed responses (to the optimal center gratings) by 15.7%. Suppression and facilitation effects were largely unaffected by phase relation between center and surround stimuli. (B) Schematic representation of how increasing the contrast of a center stimulus alone can decrease responses at very high contrast levels ('contrast supersaturation'). This suggests that the excitatory portion of the classical RF can become inhibitory. (C) Schematic representation of contrast-dependent length-tuning. Many V1 cells respond optimally to oriented high-contrast stimuli of a given length. These cells exhibit 'end-stopping' or length-tuning in that responses decline for longer high-contrast stimuli. The presumed 'inhibitory end-zones' can become excitatory when stimulus contrast is reduced. At low contrasts, length summation can extend several degrees into the 'inhibitory end-zones'. Thus, the border between excitatory and inhibitory regions appears to shift with stimulus contrast. For all three receptive field effects, modulatory stimuli tend to have both the strongest facilitatory and strongest suppressive effects when oriented at the preferred orientation of the classical RF.

Table 1
Model parameters

Variable name	Excitatory cell value	Inhibitory cell value	Variable name	Excitatory cell value	Inhibitory cell value
C_m	0.5 nF	0.2 nF	g_{LGN}	3 nS	1.5 nS
g_{Leak}	25 nS	20 nS	g_{Excit}	7 nS	1.5 nS
g_{AHP}	40 nS	20 nS	g_{Inhib}	15 nS	3 nS
g_{Adapt}	3 nS	—	g_{Long}	1.2 nS	1.2 nS
E_{Excit}	0 mV	0 mV	$\rho_{peak\ Ex}$	0.1	0.1
E_{Inhib}	−70 mV	−70 mV	$\rho_{edge\ Ex}$	0	0
E_{AHP}	−90 mV	−90 mV	$d_{egde\ Ex}$	150 mm	150 mm
E_{Adapt}	−90 mV	—	$\rho_{peak\ In}$	0.06	0.06
E_{Leak}	−65 mV	−65 mV	$\rho_{edge\ In}$	0.03	0.03
$\tau_{peak\ Ex}$	1 ms	1 ms	$d_{egde\ In}$	500 mm	500 mm
$\tau_{peak\ In}$	2 ms	2 ms	$\rho_{peak\ Long}$	0.005	0.005
$\tau_{peak\ AHP}$	1 ms	1 ms	$\rho_{edge\ Long}$	0.001	0.001
$\tau_{peak\ Adapt}$	30 ms	—	$\phi_{edge\ Long}$	90°	90°

requirements of this model and to further explore input-dependent effects, we present a novel analysis method. This analysis constructs self-contained local cortical modules which exhibit the essential local and long-range behavior of the full model. Preliminary accounts of some of this work have appeared (Somers et al., 1994, 1995b).

Materials and Methods

Model Overview
The model extends our prior local circuit model of orientation selectivity (Somers et al., 1995a) by incorporating long-range intracortical excitatory connections. The present model also differs from our prior short-range model in that: excitatory cortical neurons have been extended to exhibit spike adaptation; the equations describing lateral geniculate responses have been simplified to decrease simulation time; and 10 times as many neurons have been represented. In scaling up such a nonlinear system, parameter modifications were unavoidable; however, the essential behaviors of the earlier model (i.e. orientation sharpening, amplification) persist in the present model.

Cortical Cell Models
Excitatory and inhibitory cortical neurons were modeled separately using experimentally reported input resistances, membrane time constants and firing characteristics of regular-spiking (RS) and fast-spiking (FS) neurons (Connors et al., 1982; McCormick et al., 1985). The cellular parameters used here are the same as in our prior model, with the exception that a spike-adaptation current has been added to RS neurons. This current is not important for our results; rather, we add it because it is a known and prominent feature of RS neuron physiology. Each cortical neuron was modeled as a single voltage compartment in which the membrane potential, V, was given by

$$C_m \frac{dV_i}{dt} = -\sum_{j=1}^{k} g_{ji}(t-t_{ji})[V_i(t)-E_{Excit}] - \sum_{j=k+1}^{k+l} g_{ji}(t-t_{ji})[V_i(t)-E_{Inhib}]$$
$$-g_{Leak}[V_i(t)-E_{Leak}] - g_{AHP}(t-t_{spike})[V_i(t)-E_{AHP}]$$
$$-g_{Adapt}(t-t_{spike})[V_i(t)-E_{Adapt}]$$

where the synaptic conductances generated at each postsynaptic cell i by the spiking of each presynaptic cell j (excitatory if $j \leq k$; inhibitory if $k < j \leq l$) are given by:

$$g_{ji}(t) = \bar{g}_{ji}\sum_{p}^{s_j}(t-t_p)(e/\tau_{peak})\exp[-(t-t_p)/\tau_{peak}]$$

where t_{ji} and $\bar{g}_{ji}$ describe the delay and maximal conductance change

higher average gain and threshold for the inhibitory population (McCormick et al., 1985); and differential synaptic depression/facilitation in local circuit connections (Thomson and Deuchars, 1994).

We and others (Ben-Yishai et al., 1995; Douglas et al., 1995; Somers et al., 1995a; Suarez et al., 1995) have demonstrated that consideration of short-range recurrent cortical excitatory (and inhibitory) connections yields a concise account of a broad range of experimental data on orientation and direction selectivity. Here, we extend our large-scale visual cortical model to incorporate long-range intracortical excitation and demonstrate that this model captures both the local and long-range phenomena. In order to make clear the mechanistic

produced for the synapse between cell j and cell i. The numbers of excitatory and inhibitory synapses received by cell i were k and l respectively. AMPA receptor-mediated excitatory synaptic effects and GABA$_A$ receptor-mediated synaptic inhibitory effects were implemented as linear conductance changes. After-hyperpolarization effects were spike-triggered (with delay t_{spike} = 1 ms).

The membrane parameters (see Table 1) yield membrane time constants, τ_m, of 20 ms for excitatory neurons and 10 ms for inhibitory neurons. Na$^+$-mediated spike dynamics were replaced by a time-varying firing threshold. When the membrane potential exceeded threshold, a spike was recorded, the spike threshold was elevated, an after-hyperpolarizing conductance was activated, and for excitatory neurons an adaptation conductance was activated. Baseline spike threshold value was –55 mV. Absolute refractory periods were 3 and 1 ms for RS and FS neurons. Relative refractory periods were generated by time-varying thresholds that pulsed up 10 mV on a spike and exponentially decayed to baseline with a 10 ms time constant (5 ms for FS neurons). This roughly approximates the refractory effects of Na$^+$ channel inactivation. These parameters yielded approximate fits to experimental frequency vs. current plots for cortical neurons (McCormick *et al.*, 1985).

In our prior model the distinction between RS and FS neurons was imposed simply to be consistent with known cellular physiology. Here we utilize two differences between the two cell classes as one way to create an asymmetry in the local circuitry that provides a local gain control mechanism. Fast-spiking or inhibitory neurons have higher input resistances and thus have higher current gains (greater slope of the frequency vs. current plot) than those of RS or excitatory neurons (McCormick *et al.*, 1985). Current thresholds for FS and RS neurons are similar, but inhibitory neurons receive substantially fewer synapses and presumably less synaptic current than excitatory neurons (see Table 1). Thus, we hypothesize that FS neurons have higher functional thresholds (e.g. contrast thresholds) than RS neurons. The combination of higher gain and threshold for a population of inhibitory neurons is one mechanism used in this paper to achieve a generalized gain control mechanism in the local circuitry. The essential nonlinearity here is that the ratio of local excitatory currents to local inhibitory currents evoked by a stimulus configuration should be high for low stimulus intensities and should decrease at higher stimulus intensities (see Discussion).

Model Connectivity

In constructing a model network our goals were to represent dense local intracortical circuitry and connections that traveled long cortical distances. Given the twin requirements of density and size, a network with a very large number of neurons had to be constructed. Cortical circuitry under a 3.5 × 7 mm patch of primary visual cortex was represented by a model with 20 250 spiking cortical neurons and >1.3 million cortical synapses. Whenever possible, known anatomical values, ratios and constraints were imposed on the model. Neurons were organized into a 45 × 90 grid of 'mini-columns' (e.g. Peters and Yilmaz, 1993), based on an orientation map obtained by optical recording of intrinsic signals of cat visual cortex (Toth *et al.*, 1996). Each mini-column contained four excitatory neurons and one inhibitory neuron (ratio from Gabbott and Somogyi, 1986). Both excitatory and inhibitory neurons made short-range intracortical connections, while only excitatory neurons made long-range connections. Each type of connection targeted both excitatory and inhibitory post-synaptic neurons (e.g. Beaulieu and Somogyi, 1990; McGuire *et al.*, 1991; Anderson *et al.*, 1994). Short-range connection probabilities fell linearly from ρ_{peak} to ρ_{edge} at distance d_{edge}, with ρ = 0 beyond that (see Table 1 for parameters).

As can be seen in Figure 2, excitatory connections dominate at very short distances and inhibitory connections dominate in a local ring around them. This center-surround organization is a key property of our prior model of orientation selectivity (Somers *et al.*, 1995a). Long-range excitatory neurons preferentially targeted neurons with orientation preferences similar to their own (Gilbert and Wiesel, 1989; McGuire *et al.*, 1991; Malach *et al.*, 1993). Connection probabilities varied linearly with the orientation difference between pre- and postsynaptic cells, from ρ_{peak} = 0.005 at ϕ = 0° to ρ_{edge} = 0.001 at ϕ = 90°. Results were averaged over 20 networks, each randomly constructed using the above connectivity probabilities. Responses were analyzed over the central 3 × 3

mini-columns of the model (36 excitatory neurons). This restricted population lies within an iso-orientation domain and was selected to guarantee that the orientation and position of the stimuli were optimal for classical receptive fields of the cells investigated.

Stimuli and Inputs to Cortex

Stimuli consisted of circular ('center') and annular ('surround') gratings of differing contrasts, orientations and radii. Central RF studies used a only central grating with a diameter approximately equal to the RF (1°). End-stopping studies varied this diameter. Surround studies combined a 1° diameter center stimulus with a surround annulus (1° inner diameter; 4° outer diameter). Thalamic neuron responses to these stimuli increased linearly with log contrast. LGN responses were independent of stimulus orientation, phase and spatial frequency. LGN responses were also constant over the 300 ms simulation trials. LGN cells with receptive fields located at the border between center and surround stimuli were driven in proportion to the degree each stimulus covered the cell's receceptive field. Converging thalamocortical inputs to a column were biased for a particular stimulus orientation and location (Hubel and Wiesel, 1962), and orientation selectivity was enhanced by intracortical connections (e.g. Somers *et al.*, 1995a). The pattern of preferred orientations and locations of converging thalamocortical inputs was determined from the optical map data (see Fig. 2). The average firing rate of the converging thalamocortical input to single cortical neurons was a function of stimulus orientation (θ_{cent}, θ_{surr}), contrast (%Cont$_{cent}$, %Cont$_{surr}$), size and position:

$$
\begin{aligned}
F_{thal} \;=\; & \%Cent(x,y)\cos\!\left[60°\!\left(\theta_{cent}-\theta_{pref}\right)/\theta_{hw}\right]\log(\%Contrast_{cent}) \\
& + \%Surr(x,y)\cos\!\left[60°\!\left(\theta_{surr}-\theta_{pref}\right)/\theta_{hw}\right]\log(\%Contrast_{surr})
\end{aligned}
$$

%Cent and %Surr are the percentages of converging thalamocortical afferents that are activated by the center and surround stimuli respectively. θ_{pref} and θ_{hw} are the preferred orientation of the mini-column and the half-width at half-amplitude of the orientation tuning of the convergent pattern of thalamocortical inputs. Note that stimulus phase and spatial frequency are not factors, and thus a grating stimulus is equivalent to a patch of oriented bars of the same size, contrast and orientation. Thalamocortical response rates were converted into spikes using 10 independent Poisson processes. Cortical magnification was 1 mm/deg and each thalamic neuron projected to cortical neurons over an area of 0.8 mm^2 (Humphrey *et al.*, 1985).

Local Circuit Module Simulations

Local circuit modules were composed of 200 excitatory and 50 inhibitory neurons each with cellular equations and parameters identical to those in the full model (see cortical cell model method above). Short-range connections were made between cells in a module. In addition, cells of the module received excitatory external inputs that represented the sum of the thalamocortical and long-range intracortical inputs. For a given stimulus condition, all excitatory cells received one input value and all inhibitory cells received another. Module responses were obtained by computer simulation of this local circuit with different levels of input to the excitatory and inhibitory cells. Responses were measured for 961 input combinations (grid points). Each response averages over 40 trials with stimulus durations of 250 ms. The connection probabilities within this module were $\rho_{excit-excit}$ = 0.0044, $\rho_{excit-inhib}$ = 0.0044, $\rho_{inhib-excit}$ = 0.0125, $\rho_{inhib-inhib}$ = 0.025. The synaptic strengths were as in the full model above. In order to compare predictions of the module to the responses of the full model, external inputs to the module were extracted from simulations of the full model. These inputs represent the total thalamocortical and long-range intracortical input to excitatory and inhibitory cells in a 3 × 3 patch of mini-columns in the center of the model.

Two different module forms were constructed, one based on the circuitry of the full model called the gain-threshold asymmetry module and one that eliminated the threshold asymmetry but obtained qualitatively similar behavior by utilizing synaptic depression at local excitatory–excitatory synapses and synaptic facilitation at local excitatory–inhibitory synapses (Thomson and West, 1993; Thomson *et*
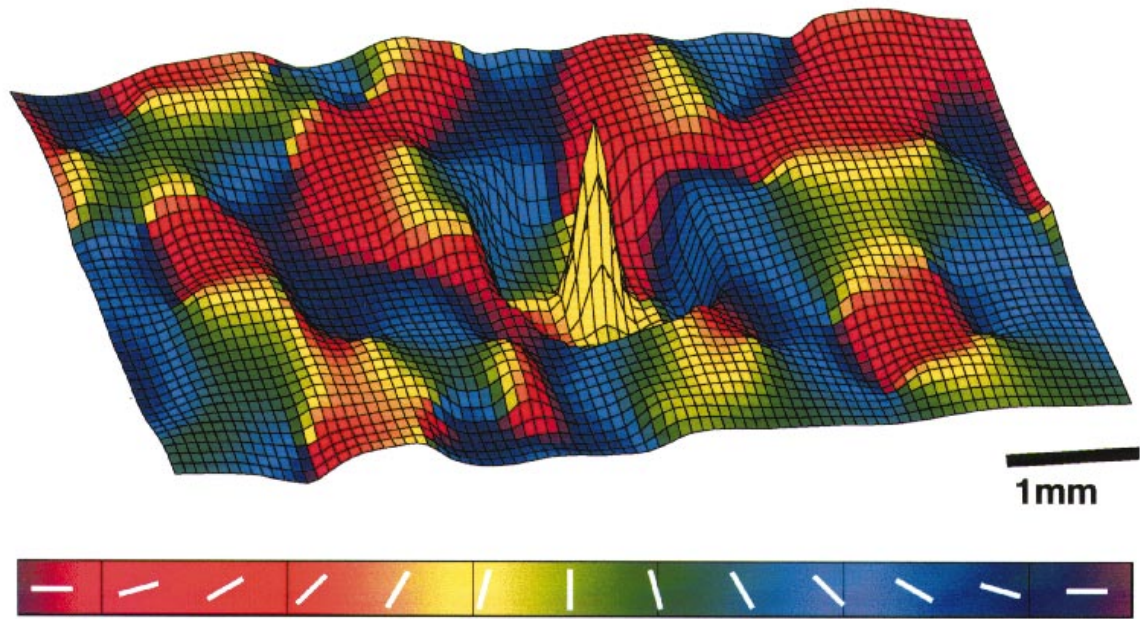
Figure 2. Connectivity of cortical circuitry in the model. The color map represents the orientation preference of each cortical mini column. The pattern of intracortical connections to cells in the central (yellow) mini-column is represented by the surface amplitude, which codes the net (Σ Excit − Σ Inhib) strength of intracortical connections from each column to the cells of the central column. Three classes of intracortical connections are included in the model: short-range excitatory, short-range inhibitory and long-range excitatory. Short-range connections are densest in the vicinity of the presynaptic cells and fall off with distance. Short-range excitatory connections are more numerous, but more spatially restricted than short-range inhibitory connections. This results in the 'Center-Surround' shape near the central orientation column. Long-range excitatory connections can span the entire circuit and preferentially target cells with similar orientation biases. Note that long-range peaks lie in yellow-colored columns. All connections target both excitatory and inhibitory neurons. Amplitude of long-range inputs has been scaled by a factor of 15 to aid visibility in the figure.

al., 1993a; Thomson and Deuchars, 1994; Abbott *et al.*, 1997; Tsodyks and Markram, 1997). This second module is called the synapse asymmetry module. Each local excitatory synapse had a synaptic efficacy, *W*, and an adaptation level, *A*, or facilitation level, *B*, associated with it:

$$W_{\text{ex−ex}} = g_{\text{ex−ex}}\big[1 - A(t)\big] \quad 0 \le A \le 1 \quad A(0) = 0$$

$$W_{\text{ex−in}} = g_{\text{ex−in}}B(t) \qquad 0 \le B \le 1 \quad B(0) = 0$$

If the presynaptic cell generated an action potential at time *t*, the peak of the conductance change was *W*. Each spike caused an increase in the adaptation and facilitation levels:

$$A[t+1] = A[t] + 0.1\big(1 - A[t]\big)$$

$$B[t+1] = B[t] + 0.1\big(1 - B[t]\big)$$

These values decayed to zero, each with time constants $\tau_A = \tau_B = 300$ ms:

$$A[t+1] = A[t]\exp(-1/\tau_A)$$

$$B[t+1] = B[t]\exp(-1/\tau_B)$$

In the simulation results presented, *A* and *B* typically ranged between 0.1 and 0.6. Connectivity probabilities in this module were simplified to $\rho_{\text{excit−excit}}$ = 0.1, $\rho_{\text{excit−inhib}}$ = 0.1, $\rho_{\text{inhib−excit}}$ = 0.1, and $\rho_{\text{inhib−inhib}}$ = 0.1. Synaptic strengths onto excitatory neurons were g_{Excit} = 2.5 nS, g_{Inhib} = 10 nS and onto inhibitory neurons were g_{Excit} = 2 nS, g_{Inhib} = 2 nS. In order to obtain identical contrast thresholds for excitatory and inhibitory neurons (for the center only stimulus), the ratio of g_{LGN} onto excitatory vs. g_{LGN} onto inhibitory neurons was 3:2. This ratio compensates for the different cellular parameters of the two classes of cells. The ratio of the long-range inputs to excitatory and inhibitory neurons was 1:1 and the magnitudes for the two surround conditions were chosen to give a clear example of the facilitation/suppression property.

Results

Model of Local and Long-range Connections In V1

We shall first show that the large-scale model of V1 (Fig. 2) explains contrast-dependent modulation of responses locally, within the classical receptive field, and then explain the long-range modulation of responses from the extraclassical receptive field.

The model captures physiological responses to oriented grating stimuli of differing contrasts presented within the classical receptive field. Model behavior is analyzed for a population of neurons lying in the central orientation domain of the model (yellow peak of Fig. 2). Figure 3*A* shows mean responses of 36 excitatory cortical neurons to oriented grating stimuli of different contrasts presented within the classical receptive field. Analysis was restricted to this population in order to ensure that analyzed cells were driven by optimally positioned and oriented center stimuli. These responses were averaged for the same set of neurons in 20 networks, each constructed with the same connectivity probability rules.

To isolate cortical effects, thalamic responses were designed to increase linearly with log contrast. The dotted lines in Figure 3*A* show contrast response curves for the cortical neurons at two different stimulus orientations when intracortical synapses are shut off and only thalamocortical inputs are active; note the linear responses above threshold. In the full model, with intracortical synapses active, cortical responses (data points and solid lines in Fig. 3*A*) exhibit a saturation nonlinearity at higher contrasts. This occurs at contrast levels for which thalamic responses have not yet saturated. Contrast saturation in the model is achieved as a network property rather than as a cellular
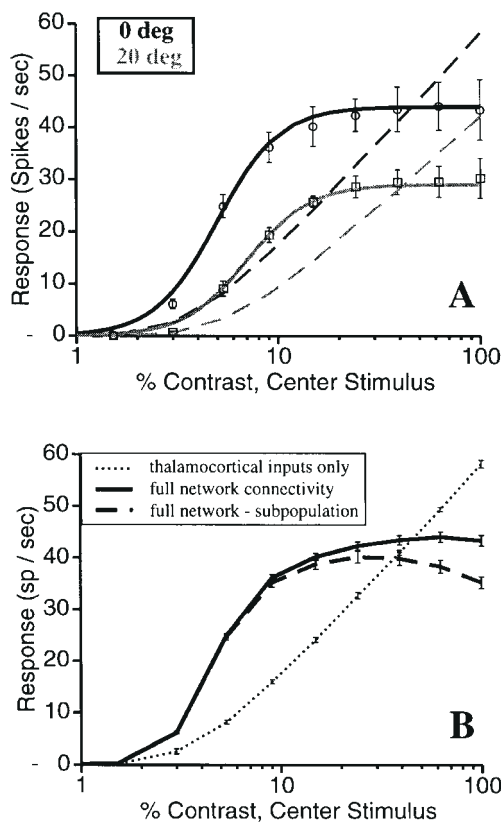
Figure 3. Contrast response functions of model. (A) Mean firing rates of 36 excitatory neurons in the central 3 × 3 columns of the model to different levels of stimulus contrast (20 trials; error bars show standard deviation). Grating stimuli were shown at the preferred orientation (black curves) and 20° off of preferred (gray curves). Data points and solid curves display responses of the full model circuit. Dashed curves display responses of the same cells when intracortical connections were silenced and only thalamocortical inputs were active. Cortical inputs strongly amplify responses to low suprathreshold contrasts, but attenuate responses to high contrasts (compare solid to dashed). Cortical circuitry provides saturating responses with different plateaus for different orientations. Solid curves fit the simulation data using a hyperbolic function $R = R_{max}C^\gamma/(C_{50}^\gamma + C^\gamma)$ (Albrecht and Hamilton, 1982). $\gamma = 2.8$ for both curves and $C_{50} = 5$ and 7% for preferred and 20° respectively. Cortical inputs also sharpen orientation selectivity. (B) For a subpopulation (18/36) of these neurons, responses decline at high contrasts (dashed line). This is called 'supersaturation'. Solid and dotted lines replot results from A (with standard error bars).

property. Responses at saturation are a mere fraction of the maximal responses of these neurons to an injected current (e.g. 40 vs. 300 imp/s). Moreover, saturation response levels vary with stimulus orientation. These simulation results were well fit (solid curves) by hyperbolic contrast response functions, $R = R_{max}C^\gamma/ (C_{50}^\gamma + C^\gamma)$, which have been shown to provide superior fits to experimental contrast response data (Albrecht and Hamilton, 1982). Results for both orientations were fit with the same exponent (γ) of 2.8. R_{max} values were 43 and 28. Mid-level contrasts (C_{50}) were 5 and 7% for preferred and 20° respectively. Consistent with our prior model (Somers *et al.*, 1995a), cortical inputs sharpen orientation tuning (compare differences between 0° and 20° responses. Note that intracortical connections amplify responses to low-contrast stimuli at the preferred orientation, but attenuate responses to high-contrast stimuli. Contrast saturation in our model reflects a gain change in local cortical circuitry that results from an asymmetry between the properties of excitatory and inhibitory neurons. Inputs from inhibitory neurons grow proportionally stronger at high levels of
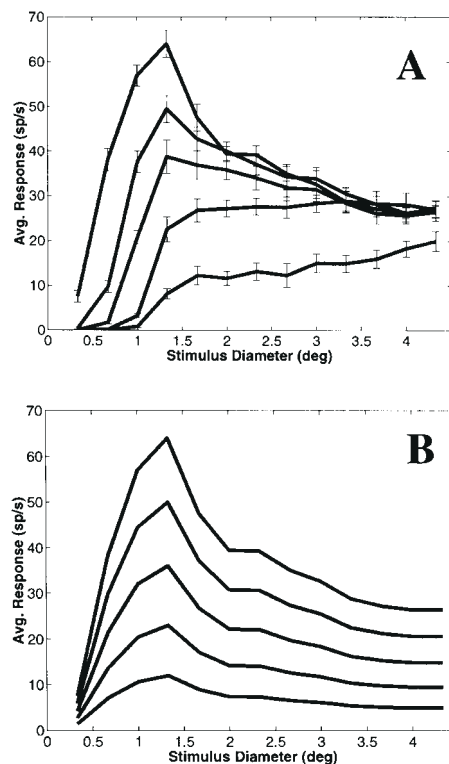

Figure 4. Preferred stimulus length increases with decreasing stimulus contrast. (A) Response vs. stimulus diameter for the same cells as Fig. 3A at five different contrast levels (60, 10, 5, 3, 2%) of the preferred orientation (10 trials, SD shown). For the highest contrast stimuli (top curve) responses are maximal for small stimuli (<1.5°) and decrease for larger stimuli. Thus the model exhibits a form of length-tuning or end-stopping. As stimulus contrast decreases (lower curves), excitatory length summation occurs for progressively larger stimuli. Note that responses to the lowest contrast are still increasing at 4°. Compare this contrast-dependence to hypothetical contrast-independent length summation curves shown in B. (B) High-contrast length response curve scaled by factors 1.0, 0.8, 0.6, 0.4 and 0.2.
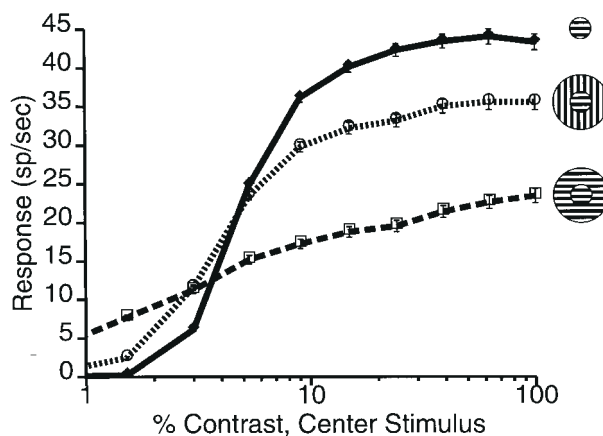

Figure 5. Facilitation and suppression by high-contrast surround stimuli. Responses of the same model neurons as in Figures 3A and 4A to varying contrast levels of a center stimulus under three fixed surround conditions: no surround (solid), high contrast cross-orientation surround (dotted), high contrast iso-orientation surround (dashed). Both surround stimuli increase responses to low contrast centers but decrease responses to high contrast center stimuli. Both facilitation and suppression effects are stronger for the iso-orientation surround.

input drive; population responses for inhibitory neurons saturate only when LGN responses saturate.
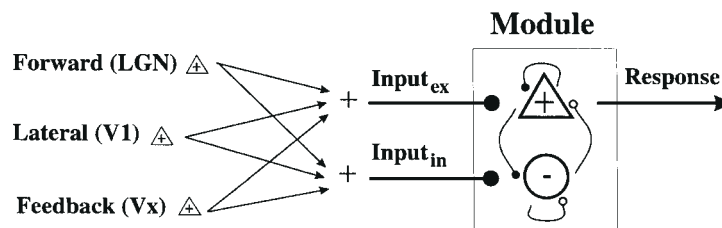
A)
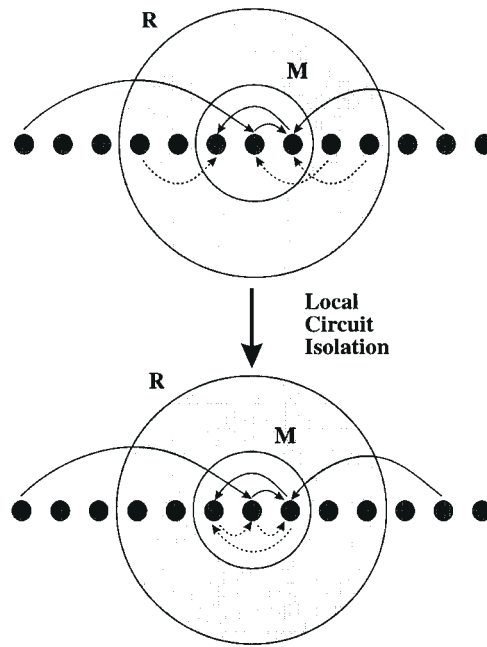
B)

Figure 6. Local circuit module construction. Behavior of a local population **M** in the full model is estimated by constructing a local circuit module composed of excitatory and inhibitory populations. (*A*) The module simplifies analysis of RF integration by capturing nonlinear local cortical interactions over a radius **R**. The module is constructed by replacing local inputs (from the gray shaded area between **M** and **R** with local inputs from within **M**. (*B*) Activity in the module depends only on thalamocortical and long-range intracortical excitatory inputs to the module. All sources of long-distance input (possibly including feedback from higher cortical areas) are summed together linearly, but inputs to excitatory and inhibitory cells remain segregated. Simulations of the local circuit module are much faster than those of the full model and thus permit exploration of local circuit responses to all possible input values.

In this work, two mechanisms are demonstrated to produce the local circuit asymmetry: (i) a population-level bias among inhibitory neurons to have higher gain and higher contrast thresholds than excitatory cells; and (ii) differential adaptation and enhancement at local intracortical excitatory synapses onto excitatory and inhibitory neurons respectively (Thomson and West, 1993; Thomson *et al.*, 1993a,b, 1995; Thomson and Deuchars, 1994). The results presented in Figures 3–8 were obtained with the first mechanism. Inhibitory neurons in the model have a higher gain because FS cells have a much higher input resistance and proportionally greater response to injected current levels than do RS cells (Connors *et al.*, 1982; McCormick *et al.*, 1985). The higher contrast threshold results because thalamic inputs provide proportionally fewer excitatory synapses onto inhibitory neurons than onto excitatory neurons. Later in this paper we demonstrate that the second mechanism obtains the same essential local circuit behavior (see Fig. 9).

For a subpopulation of modeled neurons (18/36 cells), a decline in response at high contrast was observed (see Fig. 3*B*). Li and Creutzfeldt (1984) described this behavior in detail, calling the decline 'supersaturation', because it occurs at contrast levels beyond which normal contrast saturation can be observed. Those authors suggested that supersaturation might result from reduced drive from thalamic sources at high contrasts; here, we show that a purely cortical mechanism is sufficient. The supersaturation effect, although infrequently discussed, can also be seen in other experimental reports (e.g. Bonds, 1991; Albrecht and Hamilton, 1982). Thus, for some cells, even the classical excitatory RF can have inhibitory effects when stimulation is strong.

The effects of varying stimulus length and contrast were also systematically explored within the simulations. Responses to a high-contrast visual stimulus were observed to decline beyond a characteristic preferred size (see top curve of Fig. 4*A*). Thus the model exhibited a form of length-tuning or end-stopping (Hubel and Wiesel, 1965). Consistent with experiments (e.g. Orban *et*

al., 1979; DeAngelis *et al.*, 1994), high contrast iso-orientation stimuli that extend into end-zone (or side-band) regions have potent inhibitory effects on responses to the central stimulus. In agreement with experimental findings of Jagadeesh and Ferster (1990; also Jagadeesh, 1993), the length of the excitatory receptive field increased with decreasing contrast, and at low stimulus contrasts, responses to optimal orientation gratings continued to increase monotonically. Both the experiment and simulations indicate that the borders between excitatory and inhibitory regions shift depending on the level of stimulus contrast. For comparison's sake, Figure 4*B* displays what the length tuning curves would look like if contrast-invariant length summation occurred.

While preserving classical RF properties, the model also captures paradoxical extraclassical RF modulations (Knierim and Van Essen, 1992; Sillito *et al.*, 1995; Toth *et al.*, 1996; Levitt and Lund, 1997; Polat *et al.*, 1998; Sengpiel *et al.*, 1998) The contrast of a central grating was varied under three different surround stimulus conditions: no surround; a high-contrast cross-orientation surround stimulus; and a high-contrast iso-orientation surround stimulus. The modulatory influence of 'surround' gratings on responses to optimal orientation 'center' stimuli shifts from facilitatory to suppressive as center stimulus contrast increases (Fig. 5, cf. Fig. 1*A*). Model simulations also obtain the result that both facilitation and suppression effects are strongest for iso-orientation surround stimuli (Knierim and Van Essen, 1992; Sillito *et al.*, 1995; Weliky *et al.*, 1995; Toth *et al.*, 1996; Levitt and Lund, 1997). These effects emerge from the local intracortical interactions (as will be shown below) and do not require synaptic plasticity (cf. Hirsch and Gilbert, 1991; Gilbert *et al.*, 1996) or complex cellular properties (cf. Bush and Sejnowski, 1994). This model also provides the first unified account of these classical and extraclassical RF modulations.

A Technique for Analyzing Local Circuit Behavior

The focus of this paper is to investigate how local circuitry responds to combinations of long-range input. Large-scale model simulation, while useful for addressing computational effects of neurobiological details, can be analytically cumbersome. In this section we develop a technique for analyzing large-scale recurrent models of cortical circuitry that allows us to go beyond simulation and to understand what features of the model are crucial for obtaining the phenomena of interest. The main idea is to focus on the behavior of local, densely interconnected populations of cortical neurons, and to treat them as functional units or 'modules' with a well defined input–output relationship. This analysis was inspired by anatomical studies indicating that in many cortical areas relatively punctate local circuit structures are replicated many times across the region (e.g. Mountcastle, 1978; Lund *et al.*, 1993; Peters and Yilmaz, 1993), as well as by extensive physiological evidence that local clusters of cells share many stimulus response preferences.

To understand what features of the simulation cause a cortical neuron to respond in the way it does, we have to describe three types of inputs: thalamocortical, long-range horizontal and dense local cortical projections. We suggest that much of the complexity in RF effects results from the *local* cortical inputs. Thalamocortical and long-range horizontal inputs, which together we will call 'distal inputs' (always excitatory), can be easily computed for the stimuli we study here (see below). However, local inputs arise from cells which are densely interconnected with each other and with the neuron of interest. These recurrent interactions make estimation of the local inputs

a complex task. RF analysis could be greatly simplified, provided that one were able to identify a small group of cells whose behavior is only a function of their distal inputs and the interactions among them (i.e. local interactions with cells outside that group do not have to be taken into account). It is not straightforward to do this, because anatomically the cortex is not strictly modular but instead is connected in a continuous fashion. Although an individual neuron receives the majority of its inputs from presynaptic neurons within a small radius (White, 1989; also Fig. 2), one cannot simply draw a boundary at that radius and treat the enclosed cells as a module, because cells at the periphery will receive many local projections from outside the boundary. Regardless of where one draws the anatomical boundary of a module, there will be significant interactions with cells right outside the boundary, which will force us to extend the boundary even further until it eventually encloses the entire large-scale model.

What we propose instead is an abstract functional module: a small isolated group of neurons that are interconnected in such a way as to reproduce the responses of a local neuronal population embedded in the continuously connected cortical sheet. Figure 6*A* illustrates how such a functional module can be constructed. The top diagram shows an array of orientation-tuned cells (in one dimension for clarity) in the original model, and their projections into a small area **M**. The larger circle **R** defines what is considered a local vs. a distal projection to **M**. Suppose we applied the following transformation at one location in the model: remove every projection from the shaded area into **M** (dashed arrows), and replace it with a projection from within **M** that has a randomly chosen presynaptic cell and the same postsynaptic cell (bottom diagram). What would happen if we were to run a simulation with the modified cortical model? The only cells that receive different synaptic inputs are the ones in **M**. Each cell in **M** receives exactly the same number of synapses as before; the difference is that some presynaptic cells are now in **M** instead of the being in the shaded area between **M** and **R**. However, if **R** is small enough so that the firing rates within **R** are very similar, the cells in **M** will receive the same input and thus our manipulation will not change the activity in the model. The same idea also can be applied with the assumption of nonuniform firing profiles inside **R**. Note that the activity in **M** after the transformation will depend only on distal inputs. That is, we have eliminated the problematic local projections from outside the module boundary while compensating for their effects.

The resulting functional module is illustrated in Figure 6*B*. It consists of one excitatory and one inhibitory population of neurons, homogeneously interconnected (i.e. connection probability and strength depend only on the pre- and postsynaptic cell types). Both populations are directly driven by distal excitatory input, which is the net input arriving from all areas projecting to **M**. Although we do not address the effects of inputs from higher cortical areas in this paper, the same conceptual framework can be used to analyze them. The response of the excitatory population is defined as the output of the module. The module is described completely by its input–output relationship, which is a scalar function of two-dimensional vector input – e.g. a response surface (see Fig. 7*B*).

To actually construct the module and simulate its response surface, we have to fix **M** and **R**. Clearly, the approximation is sensitive to the choice of **R**. If **R** is too large, our assumption about homogeneous firing rates within **R** will fail. If **R** is too small, what we defined as 'distal' input will actually include a

substantial amount of local input, and the module will no longer be useful since the computation of 'distal' input as a function of visual stimulus will not be possible. Furthermore, we are assuming that distal inputs are only excitatory, i.e. for a small **R** many local inhibitory projections will have to be ignored, resulting in increased approximation error. The optimal radius for **R** achieves a balance between these constraints; we have found through simulations that radius to be 300n350 μm (see Fig. 7*D* insert). The area **M** can be made very small (e.g. 1 mini-column). To avoid undesirable synchronization effects due to the increased number of connections in **M**, we increased the number of cells in **M** while preserving the average number of connections per cell. (See Local Circuit Module Simulation Methods for parameter details.)

Modular Analysis of Contrast Saturation and Surround Facilitation/Suppression

We now apply the analytical technique developed above to the phenomena observed in our large-scale simulation. To predict and to analyze the response of the full model to a given stimulus, we have to: (i) construct a functional module for the desired location in the model (the center in Fig. 2) and obtain its response surface (Fig. 7*B*); (ii) estimate the distal input (sum of thalamocortical and long-range horizontal input) to that location; and (iii) measure the height of the response surface above the two-dimensional point corresponding to the distal input to excitatory and inhibitory cells in the module.

Estimating the net distal input to the center of the model is straightforward. Assume the surround stimulus is fixed, while we gradually increase the contrast of the center stimulus. The responses in the model outside the central area will remain almost constant, and therefore the long-range horizontal inputs to the center will also remain constant. The thalamocortical drive to both excitatory and inhibitory cells in the center will increase with stimulus contrast. However, since the synapses from LGN to V1 remain fixed, the net increase in the two components of the input will be proportional, i.e. the two-dimensional input will translate along a straight line (Fig. 6*A*). The same will occur if we fix the contrast of the central stimulus, and vary the contrast or orientation of the surround – then the thalamocortical input will remain fixed, while the long-range horizontal input will vary along a straight line. In general, whenever we vary the activity of

a single input source (Fig. 6*B*), the distal input will move along a straight line in the two-dimensional input space; the slope of the line is simply the ratio of synaptic strength from that input source to the excitatory and inhibitory cells in the central area.

The prior surround modulation simulations in the full model explored the effects of increasing the contrast of a central stimulus under three fixed surround conditions. The three lines in Figure 7*A* correspond to the actual distal input to excitatory and inhibitory cells in the center of the model for the three surround conditions as center contrast is increased. Note that the linearity of the extracted distal input indicates that the module is large enough to encapsulate all local interactions (i.e. if we were to define a module with *R* = 1 cell, these lines would be rather curved, and impossible to compute without running the full simulation).

We can now predict contrast response functions simply by projecting the lines from the input plane onto the response surface and aligning their origins. The back plane of Figure 7*C* displays the predicted contrast response curves for the three surround conditions. Figure 7*D* compares the responses predicted by the module (dashed lines) to the responses of the full model (solid lines). The module clearly captures the paradoxical extraclassical receptive field effects. Thus, local circuit interactions alone (without complex cellular or synaptic changes) are sufficient to explain how a receptive field component – even an extraclassical RF region mediated by long-range connections – can shift contextually between facilitating and suppressing responses.

The effect of module size on prediction error was investigated. Contrast response functions predicted by a module of a given radius were computed for both excitatory and inhibitory populations. The average absolute error between the predicted functions and the full simulations are shown (Fig. 7*D* insert) for each radius. Error measurements weight each cell equally, thus excitatory response error contributes four times more heavily than inhibitory response error. Error is computed for both center only (solid) and center-surround (dashed) stimuli. Error is minimized for a module radius of ~350 μm. The U-shape of the function reflects a trade-off between two sources of error: neglecting some inhibitory influences at small radii and assuming too much homogeneity across mini-columns at large module radii.

Figure 7. Center and surround effects predicted by module. (*A*) External inputs to excitatory and inhibitory populations of the full model for varying center contrast under the three surround conditions (red, center only; cyan, cross-orientation surround; dark blue, iso-orientation surround). Increasing stimulus contrast proportionally scales the input to the two populations and thus forms a line. Surround stimulus inputs translate the contrast input line. Long-range inputs are less biased toward excitatory cells than are thalamocortical inputs. Note that these inputs are very nearly linear. (*B*) Mean response of module excitatory population to all levels of input to the two populations. Note that inputs are in synaptic conductance units and outputs are in spikes/s. Responses in upper right region are clipped in order to increase plot resolution in the area of interest. (*C*) Contrast response functions predicted by module are obtained by projecting input lines of *A* onto surface of *B* and then aligning the origins at zero contrast (see back plane). (*D*) Module predictions (dashed lines) closely approximate the full model responses (solid lines) for all conditions. Thus both suppressive and facilitatory extraclassical RF modulations are captured within the local cortical circuitry. The effect of module radius choice on prediction accuracy is shown in the insert. Error is minimized for a module radius of ~350 μm.

Figure 8. Piecewise linear approximation of excitatory module surface. Facilitation-suppression effects can be captured even by a simple module composed of one excitatory and one inhibitory neuron, each with threshold-linear cellular response properties and with linear interactions between the neurons. Such a module generically produces a surface that consists of: region A, where excitatory response is weak and inhibitory neurons are active; region B, where excitatory neurons are active and inhibitory responses are weak; and region C, where both populations are active. The surface in Figure 7*B,C* can be seen as a smoothed version of this surface. Any contrast input line which projects onto regions B and C will generate a response function with high gain at low contrast and low gain at high contrasts. Depending on the balance between local excitatory and inhibitory synaptic strengths and the ratio of the thalamocortical inputs to the two populations, saturating or supersaturating contrast response functions can be obtained. Long-range inputs which translate the input line up, with more relative inhibition than the thalamocortical inputs, can produce response facilitation for low-contrast centers and suppression for high-contrast center stimuli.

Figure 9. Alternative local circuit module (the 'synapse asymmetry module'). This module employs a different form of asymmetry between local excitation and inhibition yet obtains the same qualitative behavior as the module extracted directly from the full model (see Fig. 7). Here, the asymmetry between excitatory and inhibitory neuron contrast thresholds is eliminated; instead, a known asymmetry in synaptic transmission ratios is exploited. Transmission failure rates at local excitatory–excitatory synapses increase as presynaptic firing rates increase, while failure rates at local excitatory–inhibitory synapses decrease as presynaptic firing rates increase. This local circuit mechanism also achieves the long-range facilitation-suppression effects with similar inputs to those used in the module of Figure 7.
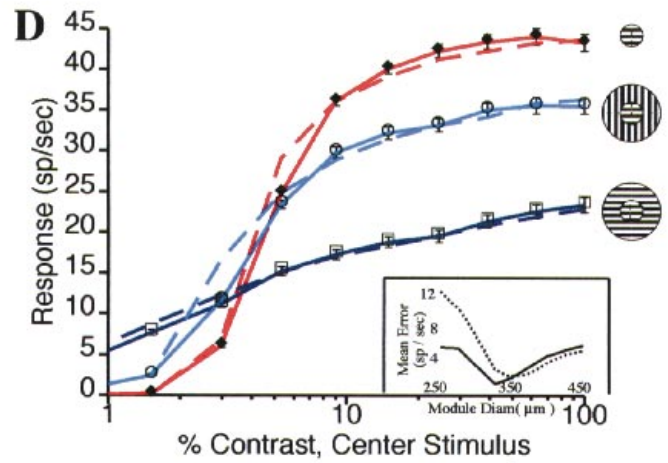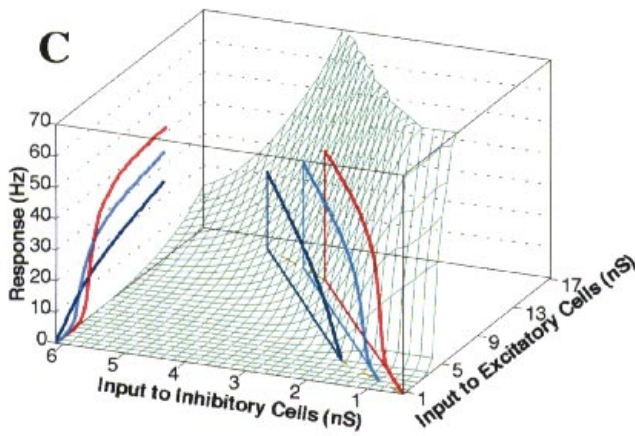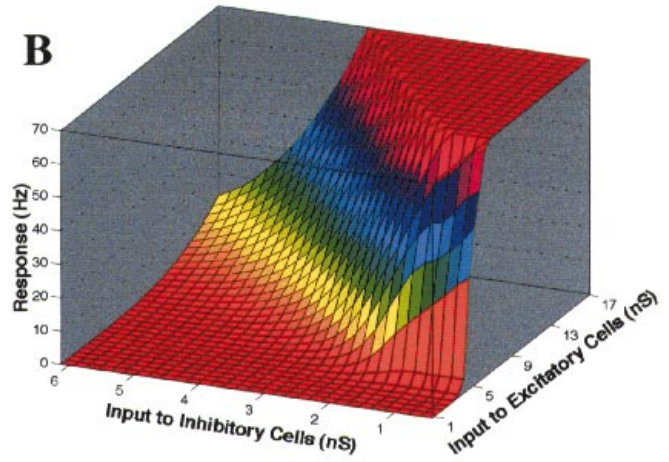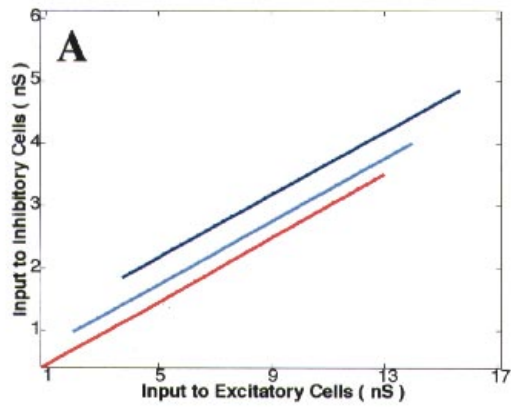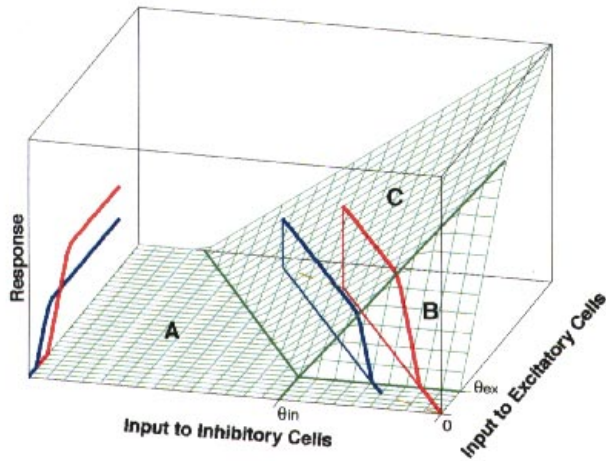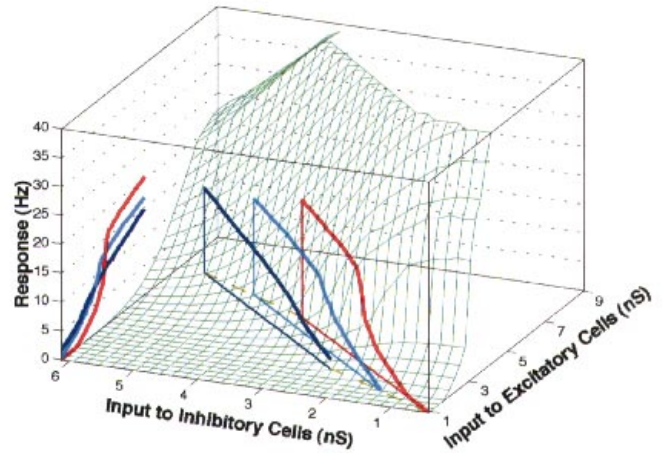
Figure 7

Figure 8

Figure 9

Analysis of Module Surface Shape

The shape of the module response surface is obviously crucial for obtaining our results. In this section we present a mathematical analysis of the features of the response surface. Here we construct a greatly simplified module consisting of a population of one excitatory and one inhibitory neuron with threshold-linear responses and linear interactions. Excitatory and inhibitory neurons have thresholds θ_{ex}, θ_{in}. Above threshold, responses increase with gains (or slopes) K_{ex}, K_{in}. Total afferent inputs to the two cells are the sum of the thalamic and long-range inputs:

$$I_{ex} = M_t T_{ex} + M_h H_{ex}$$

$$I_{in} = M_t T_{in} + M_h H_{in}$$

where M_t, M_h are thalamic and long-range horizontal firing rates, and T_{ex}, T_{in}, H_{ex}, H_{in} are the corresponding synaptic efficacies. In addition, the module cells are interconnected. The synaptic weights among excitatory (e) and inhibitory (i) cells in the module are W_{ee}, W_{ei}, W_{ie}, W_{ii}. The mean firing rates in the module can then be expressed by the following piecewise-linear system of equations:

$$M_{ex} = K_{ex}(I_{ex} + W_{ee}M_{ex} - W_{ie}M_{in} - \theta_{ex})$$

$$M_{in} = K_{in}(I_{in} + W_{ei}M_{ex} - W_{ii}M_{in} - \theta_{in})$$

The response surface in Figure 8, $M_{ex}(I_{ex}, I_{in})$, is obtained from the above system and has the same shape for a very broad range of parameter values. The surface can be divided into three regions: region A, where inhibitory responses are strong and excitatory responses are weak; region B, where excitatory responses are strong and inhibitory are weak; and region C, where both are strong and competing. Any straight line in the input plane which projects onto the surfaces of regions B and C will activate a form of gain control; response gains within region C arise more slowly than in region B.

Response saturation occurs when the input line crosses region B and is parallel to the contours in region C, i.e. $\theta_{in}/\theta_{ex} > T_{in}/T_{ex} = (W_{ii} + 1/K_{in})/W_{ie}$ (shown with red curve). In other words, saturation occurs when inhibition balances excitation. Supersaturation results from increasing the slope of the contrast input line, so that $T_{in}/T_{ex} > (W_{ii} + 1/K_{in})/W_{ie}$. That is, super-saturation occurs when inhibition overcompensates for excitation. These effects depend on the relative balance of local excitatory and inhibitory synaptic strengths as well as on the relative proportions of the thalamic drive. The surround facilitation/suppression effect (compare blue curve to red curve) is obtained when the translation vector resulting from surround stimulation has a greater slope than the contrast input line, i.e. $H_{in}/H_{ex} > T_{in}/T_{ex}$. Thus, the biphasic surround effect requires long-range excitatory connections to be less biased toward excitatory local cells than are the thalamocortical inputs. Although this simplified module neglects driving force nonlinearities and response smoothing around threshold (see Fig. 3A, thalamocortical inputs alone), it is sufficient to capture the paradoxical extraclassical RF effects; moreover, it has revealed the requirements for achieving this effect.

The response surface for the actual module (Fig. 7C,D) is essentially a smoothed version of this piecewise-linear surface (Fig. 8), which is to be expected since integrate-and-fire neurons have approximately threshold-linear feedforward responses (see Fig. 3A, dashed lines). As for the piecewise-linear module, the

key for obtaining both phenomena is the existence of region B, in which excitatory neurons respond relatively strongly while local inhibitory inputs are weak. Region B exists here because thalamocortical inputs, on average, will drive excitatory neurons at a lower input level than that required to drive inhibitory neurons above threshold. This corresponds to the prediction that inhibitory neurons, on average, have a higher contrast threshold than do excitatory neurons. Note that while the *injected current* threshold is lower for inhibitory neurons than for excitatory neurons in our model, the *contrast* threshold for inhibitory neurons is higher because thalamocortical connections are strongly biased toward excitatory neurons. In simulations of our full model, mean contrast thresholds for excitatory and inhibitory cortical neurons were 2 and 4% respectively.

An Alternative Mechanism for Obtaining the Same Module Response Surface

Having demonstrated that the paradoxical extraclassical RF effects can be explained in terms of the local cortical circuitry, we can now explore other possible neural mechanisms using local circuit modules. The simulation results presented to this point depend upon having a population of inhibitory neurons that, on average, have higher contrast thresholds than the excitatory population. This mechanism is conceptually simple, but it is not the only form of local circuit mechanism which can support these behaviors. The essential behaviors were obtained in a different local circuit in which thalamocortical inputs drive excitatory and inhibitory neurons above threshold (both 1 and 5 Hz above baseline criteria) at the same contrast levels. The necessary asymmetry in the module was obtained by modulating the efficacies of the short-range excitatory synapses onto excitatory and inhibitory neurons. Thomson and colleagues (Thomson and West, 1993; Thomson *et al.*, 1993a; Thomson and Deuchars, 1994) and others (Abbott *et al.*, 1997; Tsodyks and Markram, 1997) have reported, based on dual intracellular recordings, that synaptic transmission rates between excitatory neurons decline as the presynaptic neuron firing rate increases. Conversely, synaptic transmission from excitatory to inhibitory cortical neurons increases as presynaptic neuron firing rates increase (Thomson *et al.*, 1993b, 1995). These changes in synaptic efficacy were modeled as time varying synaptic strengths (see Materials and Methods).

Figure 9 demonstrates that this mechanism generates a local circuit module with equivalent properties to the gain-threshold asymmetry module (cf. Fig. 7C). Thus, these simulations demonstrate two local circuit mechanisms for which local inhibitory inputs grow at a higher rate than local excitatory inputs given proportionally increasing levels of external drive to the two populations.

Discussion

In this paper, we have demonstrated that RF influences may contextually switch between excitatory and inhibitory in a circuit with fixed cellular and synaptic properties. These effects appear paradoxical when RF integration is studied at the single cell level, yet are straightforward when RF integration is studied at the local circuit level. This work, for the first time, draws a connection between several paradoxical phenomena: two contrast-dependent effects within the classical RF (contrast supersaturation and contrast-dependent length tuning) and a contrast-dependent effect involving extraclassical RF influences. Using detailed computer simulations we have demonstrated that

all three phenomena could be explained by the same *local* circuit model.

In addition, we have presented an analytical technique for studying local circuit interactions within a closed system. This modular analysis provides accurate quantitative predictions of the large-scale model simulations and conclusively shows that local circuitry alone is sufficient to account for the paradoxical phenomena. In addition, this analysis clarifies the requirements for obtaining these effects, the foremost of which is an asymmetry between excitatory and inhibitory local circuit responses. The modular analysis was also employed to demonstrate an alternative local circuit mechanism which obtains the necessary asymmetry. Given the nonlinearity and complexity of local circuit models, such analytical techniques are essential if local circuit approaches are to have general application. This work also advances our computational understanding of how local cortical circuitry may serve as a functional module (e.g. Szentagothai, 1975; Mountcastle, 1978; Rakic, 1988; Douglas *et al.*, 1989; Lund *et al.*, 1993). Our analysis suggests that functional modules operate on a spatial scale that is intermediate to mini-columns (~50 μm; Peters and Sethares, 1991, 1996) and hyper-columns (~1 mm; Hubel and Wiesel, 1962).

Receptive Field Integration Performed by Local Cortical Circuitry

The present paper contributes to a growing body of work which studies RF integration at the level of the local cortical circuitry rather than at the level of the single neuron (e.g. Douglas and Martin, 1991a; Fregnac and Debanne, 1993; Douglas *et al.*, 1995; Somers *et al.*, 1995a; Stemmler *et al.*, 1995; Suarez *et al.*, 1995; Salinas and Abbott, 1996). The notion of a RF that emerges here treats the contribution from each RF location as a two-dimensional vector, with component inputs to local excitatory and local inhibitory cells. The relative contributions (or vector angle) are fixed by the anatomy (i.e. number and efficacy of synapses onto excitatory and inhibitory cells), while the magnitude varies with stimulus strength. The two input components activate a set of nonlinear interactions within the local circuit in an amplitude-dependent manner, in which the ratio of inhibitory to excitatory influence grows proportionally stronger as the overall stimulus drive (i.e. contrast, spatial extent) increases. This representation has superior predictive power over simpler models provided that the ratio of input to local excitatory and to local inhibitory cells (i.e. vector angle) changes across RF positions. Here, we have suggested that the drive to inhibitory inputs is relatively stronger at large distances from the receptive field center. We wish to suggest that the input ratio (vector angle) varies smoothly as a function of distance from RF center. This, combined with a gain control mechanism, permits the size of the classical RF to vary inversely with the level of drive.

Local Circuit Asymmetry

The dynamic RF effects demonstrated here rely on an asymmetry between excitatory and inhibitory inputs in the local cortical circuitry. The critical property is that net inhibitory local circuit influences grow stronger at a greater rate than that of local excitatory influences as external drive levels increase. This idea is also supported by electrical stimulation experiments in slices of visual cortex (Hirsch, 1995; Weliky *et al.*, 1995). We have proposed two specific mechanisms for achieving this local circuit asymmetry. The first is to utilize inhibitory neurons which, as a population, have higher response gain and higher

contrast threshold than excitatory neurons. Based on cellular physiology (McCormick *et al.*, 1985), it is known that FS or inhibitory cells have much higher response gains than RS or excitatory neurons. However, the requirement for a higher-contrast threshold has not been examined experimentally and this assumption represents one experimental prediction of our model. Because this threshold difference need only occur at a population level, it is possible to achieve this result if multiple classes of inhibitory neurons, some with high thresholds and some with low thresholds, exist. Lund and colleagues (cf. Lund *et al.*, 1995) have identified several morphological classes of inhibitory neurons in V1. Our analysis suggests that high threshold inhibitory neurons play a central role in gain control.

Recent synaptic physiology studies (Abbott *et al.*, 1997; Tsodyks and Markram, 1997) indicate that rapid activity-dependent changes in synaptic efficacy at excitatory–excitatory cortical synapses may profoundly influence cortical processing. Here, we suggest that if efficacy changes at excitatory–inhibitory synapses have the opposite sign, as is suggested by the data of Thomson and Deuchars (1994), then modulation of short-range synapses is sufficient to support contextual switching effects for both local and long-range inputs to the local cortical circuitry.

Contrast Gain Control as a Circuit Property

The functional asymmetry in the local cortical circuitry provides a generalized contrast gain control mechanism that can be accessed by all input sources. At low center-driving contrasts, local cortical excitation provides strong amplification of suprathreshold inputs. As center drive levels increase, local inhibition grows to reduce the cortical amplification factor. As a result the model achieves saturating and supersaturating contrast response functions as a local circuit property. This result is consistent with experimental evidence that contrast saturation occurs when neither cellular firing rates nor synaptic inputs have reached plateau values. Thus, we suggest that the notion that excitation saturates is incorrect; rather, inhibition counterbalances excitation. The model makes the specific prediction that cortical amplification is strongest for low-contrast suprathreshold stimuli (of the preferred orientation) and that amplification decreases and may even become attenuation as contrast increases.

This local circuit form of gain control, unlike cellular or input saturation ideas, also captures spatial contrast gain effects. Excitatory RF regions are spatially restricted when the total inputs are strong, but enlarge as inputs get weaker. These expansion–contraction effects are adaptive in that they collect (excitatory) information more widely when the overall signal is weak but restrict their spatial spread when the signal from more central RF regions is stronger. It should be noted that the term 'contrast gain control' has an ambiguous meaning in the literature, referring both to instantaneous contrast saturation, as discussed here, and slower-acting contrast adaptation. Elsewhere, we have used this model structure to address contrast adaptation effects (Todorov *et al.*, 1997b).

Other Models

Contrast saturation effects have been achieved by other network models (e.g. Grossberg, 1973; Heeger, 1992, 1993; Carandini and Heeger, 1994); however, these models oversimplify cortical circuitry, effectively yoking together excitatory and inhibitory responses. Our analysis (Figs 7 and 8) makes clear that an asymmetry between excitatory and inhibitory contributions is

required in order to obtain the dynamic switching effects. These other models restrict all inputs to lie on a single line in our input plane (see Fig. 7*B*). This restriction prevents such models from achieving the full set of phenomena captured by the present model.

Extraclassical RF facilitation-suppression effects have been independently addressed by Stemmler *et al.* (1995); however, classical RF effects were neglected in that work. In contrast, our model achieves contrast saturation, length-tuning and sharp orientation tuning with different saturation levels for different orientations. This is the first time these diverse visual cortical effects have been integrated into a single model circuit. Also, the stochastic resonance mechanism suggested by Stemmler *et al.* has no experimental support in visual cortex and plays no role in the present results. Finally, the modular analysis presented here makes explicit for the first time the requirements for achieving extraclassical RF facilitation-suppression effects.

Other Phenomena

We have shown that several orientation-specific facilitation and suppression effects can be accounted for by a single mechanism. However, several related phenomena lie outside the present scope of our model. Neuronal response properties within striate cortex exhibit greater heterogeneity than is exhibited in our model. For example, some, but not all, cells exhibit strong facilitation of responses to cross-orientation center stimuli when an iso-orientation surround stimulus is presented (Sillito *et al.*, 1995; Levitt and Lund, 1997). To achieve more diverse response properties, a model has to incorporate cells receiving widely varying numbers of synapses. This was not the case here. Since we define the probability of a synaptic connection between two cells independently of all other synapses that each cell receives, this variability averages out on the cell level. Thus all cells receive very similar numbers of synapses. Elsewhere we have presented a related model (Todorov *et al.*, 1997a) which incorporated cells receiving higher numbers of local intracortical synapses and lower numbers of thalamocortical synapses; such cells exhibited stronger supersaturation, end-stopping and sensitivity to orientation contrast (Sillito *et al.*, 1995).

Co-aligned, iso-orientation surround stimuli tend to facilitate responses for both high- and low-contrast center stimuli (Kapadia *et al.*, 1995; Polat *et al.*, 1998). This effect may be related to perceptual contour integration (Grossberg and Mingolla, 1985; Field *et al.*, 1993; Polat and Sagi 1993) and may result from excitatory–excitatory connections between co-aligned, iso-orientation cell clusters (Bosking *et al.*, 1997). Long-range connections in our model are not biased for alignment-specific spatial anisotropies. Our model could achieve this facilitation by adding alignment-specific long-range inputs that are more biased to synapse onto excitatory targets than are the present alignment-nonspecific long-range inputs. To illustrate that this 'pure' facilitation could coexist with nonaligned facilitation/suppression effects in our model, consider adding a class of long-range inputs which target *only* excitatory neurons (see Fig. 7). Such input will always increase responses regardless of the local contrast gain state. Our model could similarly be extended to incorporate other specific patterns of long-range excitation, such as feedback from area V2 (Bullier *et al.*, 1996).

Notes

Address correspondence to David Somers, Ph.D. Department of Brain and Cognitive Sciences, MIT, E10–120, 79 Amherst Street, Cambridge, MA 02139, USA. Email: somers@ai.mit.edu.

References

Abbott LF, Varela JA, Sen K, Nelson SB (1997) Synaptic depression and cortical gain control. Science 275:220–224.

Albrecht DG, Geisler W (1991) Motion selectivity and the contrast-response function of simple cells in the striate cortex. Vis Neurosci 7:531–546.

Albrecht DG, Hamilton DB (1982) Striate cortex of monkey and cat: contrast response function. J Neurosci 48:217–237.

Anderson JC, Douglas RJ, Martin KAC, and Nelson JC (1994a) Synaptic output of physiologically identified spiny stellate neurons in cat visual cortex. J Comp Neurol 341:16–24.

Beaulieu C, Somogyi P (1990) Targets and quantitative distribution of GABAergic synapses in the visual cortex of the cat. Eur J Neurosci 2:296–303.

Ben-Yishai R, Bar-Or RL, Sompolinsky H (1995) Theory of orientation tuning in visual cortex. Proc Natl Acad Sci USA 92:3844–3848.

Blakemore C, Tobin EA (1972) Lateral inhibition between orientation detectors in the cat's visual cortex. Exp Brain Res 15:439–440.

Bonds AB (1991) Temporal dynamics of contrast gain in single cells of the cat striate cortex. Vis Neurosci 6:239–255.

Born RT, Tootell RBH (1991) Single-unit and 2-deoxyglucose studies of side inhibition in macaque striate cortex. Proc Natl Acad Sci USA 88:7071–7075.

Bosking WH, Zhang Y, Schofield B, Fitzpatrick D (1997) Orientation selectivity and the arrangement of horizontal connections in tree shrew striate cortex. J Neurosci 17:2112–2127.

Bullier J, Hupe JM, James A, Girard P (1996) Functional interactions between areas V1 and V2 in the monkey. J Physiol (Paris) 90:217–220.

Bush PC, Sejnowski TJ (1994) Effects of inhibition and dendritic saturation in simulated neocortical pyramidal cells. J Neurophysiol 71:2183–2193.

Carandini M, Heeger DJ (1994) Summation and division by neurons in primate visual cortex. Science 264:1333–1336.

Connors BW, Gutnick MJ, Prince DA (1982) Electrophysiological properties of neocortical neurons *in vitro*. J Neurophysiol 48:1302–1320.

DeAngelis GC, Freeman RD, Ohzawa I (1994) Length and width tuning of neurons in the cat's primary visual cortex. J Neurophysiol 71:347–374.

DeAngelis GC, Ohzawa, I, Freeman, RD (1995) Receptive field dynamics in the central visual pathways. Trends Neurosci 18:451–458 .

Douglas RJ, Koch C, Mahowald M, Martin KAC, Suarez HH (1995) Recurrent excitation in neocortical circuits. Science 269:981–985.

Douglas RJ, Martin KAC (1991a) Opening the grey box. Trends Neurosci 14:286–293.

Douglas RJ, Martin KAC (1991b) A functional microcircuit for cat visual cortex. J Physiol 440:735–769.

Douglas RJ, Martin KAC, Whitteridge D (1988) Selective responses of visual cortical neurones do not depend on shunting inhibition. Nature 332:642–644.

Douglas, RJ, Martin, KAC, Whitteridge, D (1989) A canonical microcircuit for neocortex. Neural Comput 1:480–488.

Elias S, Grossberg S (1975) Pattern formation, contrast control, and oscillations in the short-term memory of shunting on-center off-surround networks. Biol Cybernet 20:69–98.

Ferster, D, Jagadeesh, B (1992) EPSP-IPSP interactions in cat visual cortex studied with *in vivo* whole-cell patch recording. J Neurosci 12:1262–1274.

Field DJ, Hayes A, Hess RF (1993) Contour integration by the human visual system: evidence for a local 'association field'. Vis Res 33:173–193.

Fregnac Y, Debanne D (1993) Potentiation and depression in visual cortical neurons: a functional approach to synaptic plasticity. In: Brain mechanisms of perception and memory: from neuron to behavior (Ono T, Squire L, Raichle ME, Perrett DI, Fukuda M, eds), pp. 533–561. Oxford: Oxford University Press.

Gabbott PLA, Somogyi P (1986) Quantitative distribution of GABA-immunoreceptive neurons in the visual cortex (area 17) of the cat. Exp Brain Res 61:323–331.

Gilbert CD (1992) Horizontal integration and cortical dynamics. Neuron 9:1–13.

Gilbert CD, Das A, Ito M, Kapadia M, Westheimer G (1996) Spatial integration and cortical dynamics. Proc Natl Acad Sci USA 93:615–622.

Gilbert CD, Wiesel TN (1983) Clustered intrinsic connections in cat visual cortex. J Neurosci 3:1116–1133.

Gilbert CD, Wiesel TN (1989) Columnar specificity of intrinsic horizontal and corticocortical connections in cat visual cortex. J Neurosci 9:2432–2442.

Grinvald A, Lieke EE, Frostig RD, Hildesheim R (1994) Cortical point-spread function and long-range lateral interactions revealed by real-time optical imaging of macaque monkey primary visual cortex. J Neurosci 14:2545–2568.

Grossberg S (1973) Contour enhancement, short-term memory, and constancies in reverberating neural networks. Stud Appl Math 52:217–257.

Grossberg S, Mingolla E (1985) Neural dynamics of perceptual grouping: textures, boundaries, and emergent segmentations. Percept Psychophys 38:141–171.

Gulyas B, Orban GA, Duysens J, Maes H (1987) The suppressive influence of moving textured backgrounds on responses of cat striate neurons to moving bars. J Neurophysiol 57:1767–1791.

Hartline HK (1940) The receptive fields of optic nerve fibers. Am J Physiol 130:700–711.

Heeger DJ (1992) Normalization of cell responses in cat striate cortex. Vis Neurosci 9: 181–197.

Heeger DJ (1993) Modeling simple-cell direction selectivity with normalized, half-squared, linear operators. J Neurophysiol 70:1885–1898.

Hirsch JA (1995) Synaptic integration in layer IV of the ferret striate cortex. J Physiol 483:183–199.

Hirsch JA, Gilbert CD (1991) Synaptic physiology of horizontal connections in the cat's visual cortex. J Neurosci 11:1800–1809.

Hubel DH, Wiesel TN (1962) Receptive fields, binocular interaction and functional architecture in the cat's visual cortex. J Physiol 165:559–568.

Hubel DH, Wiesel TN (1965) Receptive fields and functional architecture in two non-striate visual areas. J Neurophysiol 41:229–289.

Hubel DH, Wiesel TN (1977) Functional architecture of macaque monkey visual cortex. Proc R Soc Lond B 198:1–59.

Humphrey AL, Sur M, Uhlrich DJ, Sherman SM (1985) Projection patterns of individual x- and y-cell axons from the lateral geniculate nucleus to cortical area 17 in the cat. J Comp Neurol 233:159–189.

Jagadeesh B, Ferster D (1990) Receptive field lengths in cat striate cortex can increase with decreasing stimulus contrast. Soc Neurosci Abstr 16:130.11.

Jagadeesh B (1993) The construction of receptive field properties of cells in the cat visual cortex from the synaptic inputs to the cortex. Ph.D. Dissertation. Northwestern University.

Jones JP , Palmer LA (1987) The two-dimensional spatial structure of simple receptive fields in cat striate cortex. J Neurophysiol 58:1187–1211

Kapadia MK, Ito M, Gilbert CD, Westheimer G (1995) Improvement in visual sensitivity by changes in local context: parallel studies in human observers and in V1 of alert monkeys. Neuron 15:843–856.

Kisvarday ZF, Martin KAC, Fruend TF, Magloczky Z, Whitteridge D, Somogyi P (1986) Synaptic targets of HRP-filled layer III pyramidal cells in the cat striate cortex. Exp Brain Res 64:541–552.

Knierim JJ, Van Essen DC (1992) Neuronal responses to static texture patterns in area V1 of the alert macaque monkey. J Neurophysiol 67:961–980.

Kuffler SW (1953) Discharge patterns and functional organization of the mammalian retina. J Neurophysiol 16:37–68.

Levitt JB, Lund JS (1997) Contrast dependence of contextual effects in primate visual cortex. Nature 387: 73–76.

Li CY, Creutzfeldt OD (1984) The representation of contrast and other stimulus parameters by single neurons in area 17 of the cat. Pflüger's Arch 401:304–314.

Lund JS, Yoshioka T, Levitt JB (1993) Comparison of intrinsic connectivity in different areas of macaque monkey cerebral cortex. Cereb Cortex 3:148–162.

Lund JS, Wu Q, Hadingham PT, Levitt JB (1995) Cells and circuits contributing to functional properties in area V1 of macaque monkey cerebral cortex: bases for neuroanatomically realistic models. J Anat 187:563–581.

Maffei L, Fiorentini A (1976) The unresponsive regions of visual cortical receptive fields. Vis Res 16:1131–1139.

Malach R, Amir Y, Harel M, Grinvald A (1993) Relationship between intrinsic connections and functional architecture revealed by optical imaging and in vivo targeted biocytin injections in primate striate cortex. Proc Natl Acad Sci USA 90:10469–10473.

McCormick DA, Connors BW, Lighthall JW, Prince DA (1985) Comparative electrophysiology of physiology of pyramidal and sparsely spiny stellate neurons of the neocortex. J Neurophysiol 54:782–806.

McGuire, BA, Gilbert, CD, Rivlin, PK, Wiesel, TN (1991) Targets of horizontal connections in macaque primary visual cortex. J Comp Neurol 305, 370–392.

Mountcastle, VB (1978) An organizing principle for the cerebral function: the unit module and the distributed system. In: The mindful brain (Edelman GM, Mountcastle VB, eds), pp. 7–50. Cambridge, MA: MIT Press.

Movshon JA, Thompson ID, Tolhurst DJ (1978) Spatial summation in the receptive fields of simple cells in the cat's striate cortex. J Physiol 283:53–77.

Nelson JI, Frost BJ (1978) Orientation-selective inhibition from beyond the classic visual receptive field. Brain Res 139:359–365.

Nelson JI, Frost BJ (1985) Intracortical facilitation among co-oriented, co-axially aligned simple cells in cat striate cortex. Exp Brain Res 61:54–61.

Orban GA, Kato H, Bishop PO (1979) Dimensions and properties of end-zone inhibitory areas in receptive fields of hypercomplex cells in cat striate cortex. J Neurophysiol 42:833–849.

Peters A, Yilmaz E (1993) Neuronal organization in area 17 of cat visual cortex. Cereb Cortex 3:49–68.

Peters A, Sethares C (1991) Organization of pyramidal neurons in area 17 of monkey visual cortex. J Comp Neurol 306:1–23.

Peters A, Sethares C (1996) Myelinated axons and the pyramidal cell modules in monkey primary visual cortex. J Comp Neurol 365:232–255.

Polat U, Sagi D (1993) Lateral interactions between spatial channels: suppression and facilitation revealed by lateral masking experiments. Vis Res 33: 993–999.

Polat U, Mizobe K, Pettet MW, Kasamatsu T, Norcìa AM (1998) Collinear stimuli regulate visual responses depending on a cell's contrast threshold. Nature 391:580–584.

Rakic P (1988) specification of cerebral cortical areas. Science 241:170–176.

Rockland KS, Lund JS (1982) Intrinsic laminate lattice connection in primate visual cortex. Science 215:1532–1534.

Roig BR, Kabara JF, Snider RK, Bonds AB (1996) Non-uniform influence from stimuli outside the classical receptive field on gain control of cat visual cortical neurons. Invest Opthalmol Vis Sci Suppl 37:2198.

Salinas E, Abbott LF (1996) A model of multiplicative neural responses in parietal cortex. Proc Natl Acad Sci USA 93:11956–11961.

Sengpiel F, Baddeley RJ, Freeman TCB, Harrad R, Blakemore C (1998) Different mechanisms underlie three inhibitory phenomena in cat area 17. Vis Res (in press).

Sillito AM, Grieve KL, Jones HE, Cudeiro J, Davis J (1995) Visual cortical mechanisms detecting focal orientation discontinuities. Nature 378:492–496.

Somers DC, Nelson SB, Sur M (1994) Effects of long-range connections on gain control in an emergent model of visual cortical orientation selectivity. Soc Neurosci Abstr 20:646.7.

Somers DC, Nelson SB, Sur M (1995a) An emergent model of orientation selectivity in cat visual cortical simple cells. J Neurosci 15:5448–5465.

Somers DC, Toth LJ, Todorov E, Rao SC, Kim D-S, Nelson SB, Siapas AG, Sur M (1995b) Variable gain control in local cortical circuitry supports context-dependent modulation by long-range connections. In: Lateral interactions in the cortex: structure and function (Sirosh J, Miikkulainen R, Choe Y, eds). Austin, TX: University of Texas Press WWW electronic book: http://www.cs.utexas.edu/users/nn/lateral_interactions_book/coverhtml.

Stemmler M, Usher M, Niebur E (1995) Lateral interactions in primary visual cortex: a model bridging physiology and psychophysics. Science 269:1877–1880.

Suarez H, Koch C, Douglas R (1995) Modeling direction selectivity of simple cells in striate visual cortex within the framework of the canonical microcircuit. J Neurosci 15:6700–6719.

Swindale NV (1990) Is the cerebral cortex modular? Trends Neurosci 13:487–492.

Szentagothai J (1975) The 'module-concept' in cerebral cortex architecture. Brain Res 95:475–496.

Thomson AM, Deuchars J (1994) Temporal and spatial properties of local circuits in neocortex. Trends Neurosci 17:119–126.

Thomson AM, West DC (1993) Fluctuations in pyramid-pyramid excitatory postsynaptic potentials modified by presynaptic firing pattern and postsynaptic membrane potential using paired intracellular recordings in rat neocortex. Neuroscience 54:329–346.

Thomson AM, Deuchars J, West DC (1993a) Large, deep layer pyramid-pyramid single axon EPSPs in slices of rat motor cortex display paired pulse and frequency-dependent depression, mediated presynaptically and self-facilitation, mediated postsynaptically. J Neurophysiol 70:2354–2369.

Thomson AM, Deuchars J, West DC (1993b) Single axon excitatory postsynaptic potentials in neocortical interneurons exhibit pronounced paired pulse facilitation. Neuroscience 54:347–360.

Thomson AM, West DC, Deuchars J (1995) Properties of single axon excitatory postsynaptic potentials elicited in spiny interneurons by action potentials in pyramidal neurons in slices of rat neocortex. Neuroscience 69:727–738.

Todorov EV, Siapas AG, Somers DC (1997a) A model of recurrent interactions in primary visual cortex. In: Advances in neural information processing systems (Mozer MC, Jordan MI, Petsche T, eds), Vol. 9, pp. 118–124. Cambridge MA: MIT Press.

Todorov EV, Siapas AG, Somers DC, Nelson [ ] (1997b) Modeling visual cortical contrast adaptation effects. In: Computational neuroscience, trends in research 1997 (Bower JM, ed), pp. 525–531. New York: Plenum Press.

Toth LJ, Rao SC, Kim D-S, Somers D, Sur M (1996) Subthreshold facilitation and suppression in primary visual cortex revealed by intrinsic signal imaging. Proc Natl Acad Sci USA 93:9869–9874.

T'so DY, Gilbert CD, Wiesel TN (1986) Relationship between horizontal interactions and functional architecture in cat striate cortex as revealed by cross-correlation analysis. J Neurosci 6:1160–1170.

Tsodyks MV, Markram H (1997) The neural code between pyramidal neurons depends on neurotransmitter release probability. Proc Natl Acad Sci USA 94:719–723.

Weliky M, Kandler K, Fitzpatrick D, Katz LC (1995) Patterns of excitation and inhibition evoked by horizontal connections in visual cortex share a common relationship to orientation columns. Neuron 15:541–552.

White EL (1989) Cortical Circuits, pp 46–82. Boston, MA: Birkhauser.